Turk Neurosurg, 2023

Original Investigation

DOI: 10.5137/1019-5149.JTN.41743-22.2

Received: 13.08.2022
Accepted: 05.12.2022

Published Online: 23.05.2023

Investigation of Demyelination and Remyelination Processes of the Compressed Optic Chiasm: An Experimental Model

Atakan EMENGEN[1], Ihsan ANIK[2], Sibel KOKTURK[3], Ayse KARSON[4], Eren YILMAZ[2], Ece BASARAN[5], Melih CAKLILI[6], Yonca ANIK[7], Sureyya CEYLAN[8], Burak CABUK[2], Savas CEYLAN[2]

[1]Kocaeli State Hospital, Department of Neurosurgery, Kocaeli, Turkey
[2]Kocaeli University, Department of Neurosurgery, Pituitary Research Center, Kocaeli, Turkey
[3]Istanbul University, Faculty of Medicine, Department of Histology and Embryology, Istanbul, Turkey
[4]Kocaeli University, Faculty of Medicine, Department of Physiology, Kocaeli, Turkey
[5]Kocaeli University, Medical Faculty, Department of Ophthalmology, Izmit, Kocaeli, Turkey
[6]Taksim Education and Research Hospital, Department of Neurosurgery, Istanbul, Turkey
[7]Kocaeli University, Faculty of Medicine, Department of Radiology, Kocaeli, Turkey
[8]Kocaeli University, Faculty of Medicine, Department of Histology and Embryology, Kocaeli, Turkey

Corresponding author: Atakan EMENGEN ✉ dratakanemengen@gmail.com

To watch the surgical videoclip, please visit http://turkishneurosurgery.org.tr/uploads/jtn-41743-video.mp4

ABSTRACT

AIM: The most important symptoms of pituitary adenomas and the main indications for surgical intervention are loss of visual field and visual acuity. Structural and functional changes in axonal flow have been reported due to surgical decompression after operations for sellar lesions, and recovery rates remain unknown. Using an experimental model similar to the compression of pituitary adenomas on the optic chiasm, we demonstrated demyelination and remyelination of the optic nerve histologically using electron microscopy.

MATERIAL and METHODS: The animals were fixed to a stereotaxic device under deep anesthesia, and a balloon catheter was placed under the optic chiasm through the burr hole opened in front of the bregma according to the brain atlas. According to the amount of pressure applied, the animals were divided into five groups: demyelination and remyelination groups. The fine structures of the tissues obtained were evaluated using electron microscopy.

RESULTS: Each group contained eight rats. We found a significant difference in the severity of degeneration when comparing group 1 with group 5 ($p<0.001$); there was no degeneration in group 1 rats and severe degeneration in all of the group 5 rats. Oligodendrocytes were found in all rats in group 1 and none of the rats in no group 2. The nuclei were preserved in the group 1 rats but damaged in all of the group 5 rats. There were no lymphocytes or erythrocytes in group 1 and all positives in group 5.

CONCLUSION: This technique, which induced degeneration without causing damage to the optic nerve with toxic or chemical agents, revealed Wallerian degeneration similar to tumoral compression. After compression relief, the optic nerve remyelination process can be better understood, particularly for sellar lesions. In our opinion, this model may guide future experiments to identify protocols to induce and accelerate remyelination.

KEYWORDS: Degeneration, Optic chiasm, Optic nerve, Pituitary tumors, Remyelination

ABBREVIATIONS: CNS: Central nervous system, **DTI:** Diffusion tensor imaging, **EM:** Electron microscopy, **OCT:** Optic coherence tomography

Atakan EMENGEN : 0000-0002-6853-1540
Ihsan ANIK : 0000-0003-2567-7969
Sibel KOKTURK : 0000-0001-5636-3300
Ayse KARSON : 0000-0003-4909-4012
Eren YILMAZ : 0000-0002-5911-7268
Ece BASARAN : 0000-0003-4908-7349
Melih CAKLILI : 0000-0002-4405-0566
Yonca ANIK : 0000-0002-6768-2574
Sureyya CEYLAN : 0000-0002-7889-2040
Burak CABUK : 0000-0003-1198-3869
Savas CEYLAN : 0000-0002-2747-8907

INTRODUCTION

Visual field loss occurs after chiasmal compression in pituitary adenomas, the most common brain tumors in the sellar region, if the extension toward the superior of the sella is observed (7,11). In this case, it causes blurred vision and narrowing of peripheral vision in patients (10,26). The most important symptoms of pituitary adenomas and the main indications for surgical intervention are loss of visual field and visual acuity. Impaired signal transmission along axons indicates axonal damage caused by chiasmal lesion compression (12,21,23). Structural and functional changes in axonal flow have been reported after operations for sellar lesions due to surgical decompression (25), and recovery rates remain unknown (13,17,18,24). For this reason, more experimental and clinical research is required to better understand the optic nerve regeneration process.

Myelination improves the physiological function of nerve fibers by speeding up the transmission of axon electrical signals (4). Demyelination is caused by the inhibition of myelin formation or degradation and is classified into two types: primary demyelination (30), which refers to myelin elimination without axonal destruction, and secondary demyelination, which occurs after axonal damage (14,37). CNS neural stem cells can self-renew and potentially differentiate into neurons, astrocytes, and oligodendrocytes, repairing CNS injuries (14,19,28).

In our clinical series, we performed more than 4,400 endoscopic transsphenoidal pituitary lesion surgeries and 205 giant pituitary adenomas (6). We were inspired by the fact that macroadenomas cause visual impairment and post-surgical recovery rates vary. In previous DTI studies, we demonstrated these radiologically. This experimental model was designed to demonstrate the changes in the optic nerve, which occur at the cellular level.

Because remyelination occurs after demyelination, the demyelination processes must be well understood. In this study, we used a stereotaxy device to apply compression to the optic chiasm with a balloon catheter, mimicking the chiasmal compression seen in sellar region lesions. We observed demyelination and remyelination of the optic nerve using electron microscopy.

MATERIAL and METHODS

Experimental Procedures

Animals

All experiments were performed on adult male Wistar albino rats (KOU DETAB) weighing 300 g (16–20 weeks old). The animals were housed in four cages with a 12-h light/dark cycle in a temperature-controlled (23°C ± 2°C) room. Food and water were freely available. Animals were housed in single cages for follow-up during the postoperative period. All research and animal care procedures were performed in accordance with international guidelines for the use of laboratory animals and were approved by the Animal Experiments Local Ethics Committee at Kocaeli University (KOÜ HADYEK 2/2-2020; 27.02.2020).

Stereotaxic Surgery

The animals were deeply anesthetized with an intraperitoneal injection of ketamine (10 mg/kg) and xylazine (2 mg/kg). Following the pain tests, rats were placed in a stereotaxic device (Stoelting, Wood Dale, IL) in a neutral position from external ears and front teeth in a flat position relative to the skull. After a local anesthetic agent was applied subcutaneously, the rat was positioned according to the brain atlas (Paxinos & Watson, 2007), and a 14- to 15-mm linear incision was made from the middle of both optic spheres to the posterior of the bregma.

After lateral scraping of the periosteum, the bregma was located, and the stereotaxy device was calibrated for each animal. A burr hole was opened with a high-speed electric drill at 6.2-mm anterior to the bregma (where the two optic nerves enter the optic canal according to the atlas of Paxinos & Watson, 2007).

Based on distance measurements obtained during cadaver experiments, 7 mm was measured from the burr hole entrance to the optic chiasma level. All catheters used in the severe pressure group were simultaneously calibrated with 2 mL of saline. Catheters were inserted from the burr hole level perpendicular to the skull base between the two hemispheres, and after reaching the skull base, they were directed 7 mm posteriorly between the two optic nerves (Video 1).

Experimental Design

The animals were divided into two groups: those with severe compression and those with mild compression. In the severe compression group, the air inside the catheter was removed with negative pressure and then inflated with 2 mL of saline under the optic chiasm (Figure 1). In the mild compression group, the catheter was not inflated and was left at the optic chiasm level. To ensure no liquid leakage, the catheter was soldered with a heat-adjustable soldering station while still fixed. The balloon was then secured beneath the skin with acrylic. In the mild compression group, the same procedures were performed, but the balloon was not inflated with saline, and a compression effect was created using the catheter's 2F size (Figure 2).

Animal Classification

Adult male Wistar albino rats were used in this study. The rats weighed an average of 300 g and were kept in standard laboratory conditions with free access to food and water. Five groups of rats were formed (Table I):

Group 1: Control group. This group underwent no surgical procedure and was decapitated while under deep anesthesia.

Group 2: Mild compression demyelination group. Demyelination was achieved in this group through compression without saline inflation after stereotaxic catheter application.

Group 3: Severe compression demyelination group. Demyelination was achieved in this group by inflating with 2 mL of saline after stereotaxic catheterization.

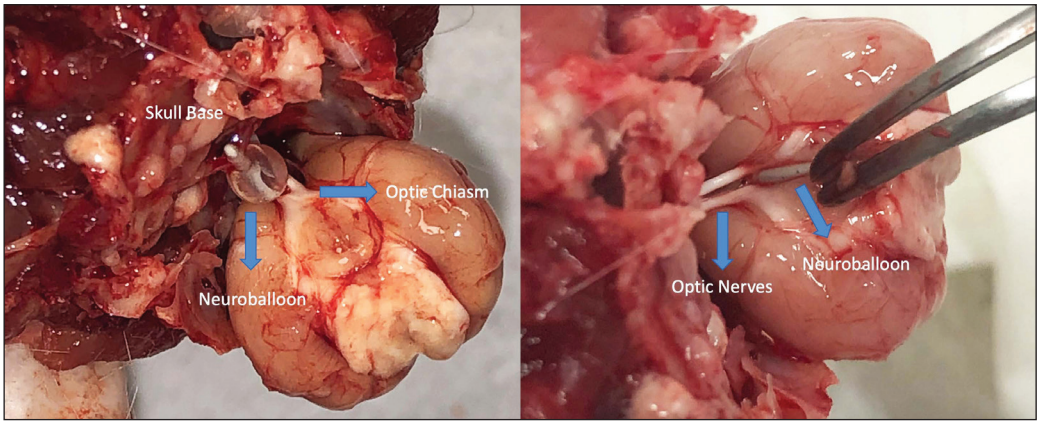

Figure 1: Posterior view of the cranium after decapitation. The catheter that has reached the optic chiasm between both optic nerves by the stereotactic method and creates severe and mild pressure under the optic chiasm.

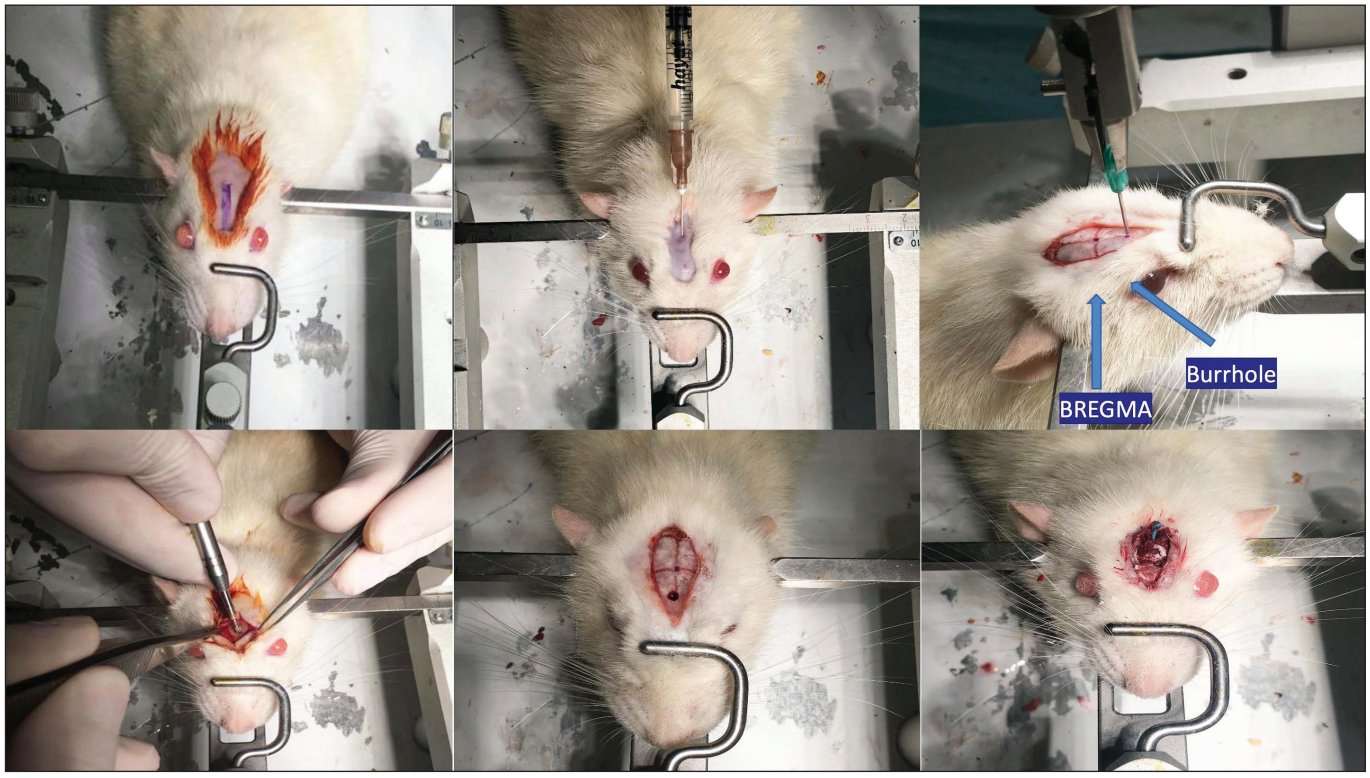

Figure 2: After the rats are fixed to the stereotaxy device, the incision line is determined, and the bregma and burr hole point are calculated. The burr hole is opened with the help of a high-speed motor from 6.2 mm in front of the bregma and fixed with acrylic after the catheter is sent.

Group 4: Mild compression remyelination group. Before removing the optic nerve, this group allowed for remyelination (after mild compression).

Group 5: Severe compression remyelination group. Before removing the optic nerve, this group allowed for remyelination (after severe compression).

The specified model was used in rats in groups 2 to 5 under sterile conditions. Previous research indicates that the demyelination process caused by optic nerve damage in rats lasts 7–10 days and the remyelination process takes 7–14 days. On the 10th day, catheters in all groups were removed under general anesthesia. The rats in groups 2 and 3 were decapitated under deep anesthesia on the same day of catheter removal. On the 10th day after catheter removal, the rats in groups 4 and 5 were decapitated under deep anesthesia to allow for myelination (Figure 3).

The skull was carefully opened, and the brain tissue was elevated superiorly from the foramen magnum. Catheter placement was controlled in groups 2 and 3, and the optic nerves and chiasm were removed from the optic canal to the ending nerves after anatomical dissection. The optic nerves were removed in their entirety and placed in test tubes containing a glyceraldehyde solution at +4°C to be examined using electron microscopy. The animals in groups

4 and 5 were decapitated 10 days after these procedures, and their optic nerves were removed and stored in tubes containing glyceraldehyde at +4°C to be examined using electron microscopy. During the experiment, six animals died in the postoperative period (three animals due to damage to the anterior cerebral artery complex and three animals due to anesthesia).

Histopathological Examination

The fine structures of the tissues obtained from each experimental group were evaluated using electron microscopy. All procedures were performed sequentially to examine the tissues under the electron microscope. The grid sections were contrasted with uranyl acetate and lead nitrate and examined under the Jeol JEM 1011 transmission electron microscope. Sections were imaged using a Mega View III digital camera and the Soft Imaging System Analysis program. Nerve fibers were examined based on the severity and degree of damage (Table II). Damaged nerve fibers were classified into three categories based on the pathological changes described above (33): mild degeneration, moderate degeneration, and severe degeneration.

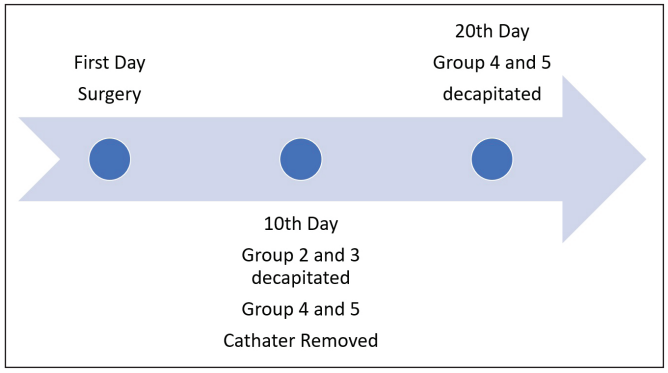

Figure 3: Experimental process.

Statistical Analysis

Statistical analysis was performed using the computer-based software program SPSS 28.0, which employed simple descriptives and frequencies. The Chi-square test, Mann–Whitney *U* test, and Kolmogorov–Smirnov tests were used to determine the significance among groups. p values of ≤0.05 were considered significant.

RESULTS

There were eight rats in group 1, seven rats in groups 2 and 4, and six rats in groups 3 and 5 (Table III). When comparing group 1 with group 5 rats, there was a significant difference in pathological findings, such as degeneration severity, oligodendrocytes, nuclei, and lymphocytes/erythrocytes ($p<0.001$). No degeneration was detected in group 1 rats, and severe degeneration was seen in all group 5 rats. Oligodendrocytes were found in all rats in group 1. Nuclei were preserved in

Table I: Groups of Rats in the Study and Number of Samples Taken

	Groups	Animal	Live Animal	Number of Glutaraldehyde Samples
Group 1	Control	8	8	8
Group 2	Mild compression demyelination group	8	7	7
Group 3	Severe compression demyelination group	8	6	6
Group 4	Mild compression remyelination group	8	7	7
Group 5	Severe compression remyelination group	8	6	6

Table II: Histopathological Examination Seen in Groups

Mild Compression Demyelination	Severe Compression Demyelination	Mild Compression Remyelination	Severe Compression Remyelination
Oligodendrocytes (+)	Oligodendrocytes (+)	Oligodendrocytes (+)	Oligodendrocytes (-)
Preserved Intracellular Organelles	Preserved/damaged Intracellular Organelles	Preserved Intracellular Organelles	Damaged Intracellular Organelles
Preserved nuclei	Preserved/damaged Nuclei	Preserved nuclei	Damaged nuclei
Lymphocytes/ erythrocytes (-)	Lymphocytes/erythrocytes (-)	Lymphocytes/erythrocytes (-)	Lymphocytes/erythrocytes (+)
Myelin Debris	Increase in Extracelular area	Myelin Debris	Severe Delamination
Delamination in Myelin Lamels		Watery Degeneration	
Dark Axon Degenerations			

Table III: Degeneration Severity and Cellular Evaluation After Electron Microscopy Examination

	Group 1	Group 2	Group 3	Group 4	Group 5	Total
Degeneration Violence						
None	8					8 (23.5%)
Medium		7	1	6		14 (41.2%)
Heavy			5	1	6	12 (35.3%)
Oligodendrocytes						
None	0	0	2	1	6	9 (26.5%)
Positive	8	7	4	6	0	25 (73.5%)
Intracellular Organelles						
Preserved	8	7	5	4	2	26 (76.5%)
Damaged	0	0	1	3	4	8 (23.5%)
Nuclei						
Preserved	8	7	3	6	0	4 (11.8%)
Damaged	0	0	3	1	6	30 (88.2%)
Lymphocytes/ Erythrocytes						
None	8	7	5	6	0	26 (76.5%)
Positive	0	0	1	1	6	8 (23.5%)

Table IV: Statistically Significance or Near Significance p Values

Pathology		**p**
Degeneration violence	Group 1 vs Group 5	<0.001
	Group 1 vs Group 3	0.003
Oligodendrocyte	Group 1 vs Group 5	<0.001
	Group 1 vs Group 3	0.069
Intracellular organelles	Group 1 vs Group 5	0.015
	Group 1 vs Group 4	0.039
Nuclei	Group 1 vs Group 5	<0.001
	Group 1 vs Group 3	0.063
Lymphocytes/Ertyhrocytes	Group 1 vs Group 5	<0.001

group 1 rats but damaged in all rats in group 5. No lymphocytes or erythrocytes were found in group 1 rats, but they were found in all group 5 rats. In terms of intracellular organelles, we found a significant difference between groups 4 and group 1 rats (p=0.039).

Degeneration was greater in group 3 rats than in group 1 rats (p=0.003). There were statistically significant differences in oligodendrocytes and nuclei between groups 1 and 3. Group 2 rats did not differ significantly from group 1 rats (Table IV).

The ultrastructural damage to the optic chiasm in the experimental groups was similar to changes in Wallerian degeneration (secondary demyelination). Ultrastructural damage resulted in three major changes: watery degeneration (axon swelling), dark axon degeneration, and demyelination.

The cytoplasm of the control group's oligodendrocytes contained numerous ribosomes, endoplasmic reticulum, and round- or oval-shaped mitochondria (Figure 4).

The mild compression demyelination group vacuolized swollen axons (watery degeneration) and myelin debris inside or outside the myelin (Figure 5A). Vacuolization, delamination, axon narrowing, and damage were observed between the myelin and axolemma of the axon (Figure 5B, C). Delamination, demyelination, destruction, and loss of myelin lamellae (Figure 5A) and dark axon degenerations were observed (Figure 5B). Oligodendrocytes exhibit large and excessive cytoplasm vacuolation and damaged mitochondria when compared with the control group (Figure 5D).

Severe nerve fiber disorganization was observed in the severe compression demyelination group (Figure 6). We observed vacuolized irregularly shaped axons, myelin debris inside or outside the myelin, and vacuolized axons. Numerous swollen and dark axon degenerations and an increase in extracellular space were also observed (Figure 7). A large number of vacuolations and damaged mitochondria were found in oligodendrocytes, which were reduced in number when compared with the control and mild demyelination and remyelination groups.

We found severe nerve fiber disorganization in the mild compression remyelination group (Figure 8). There were

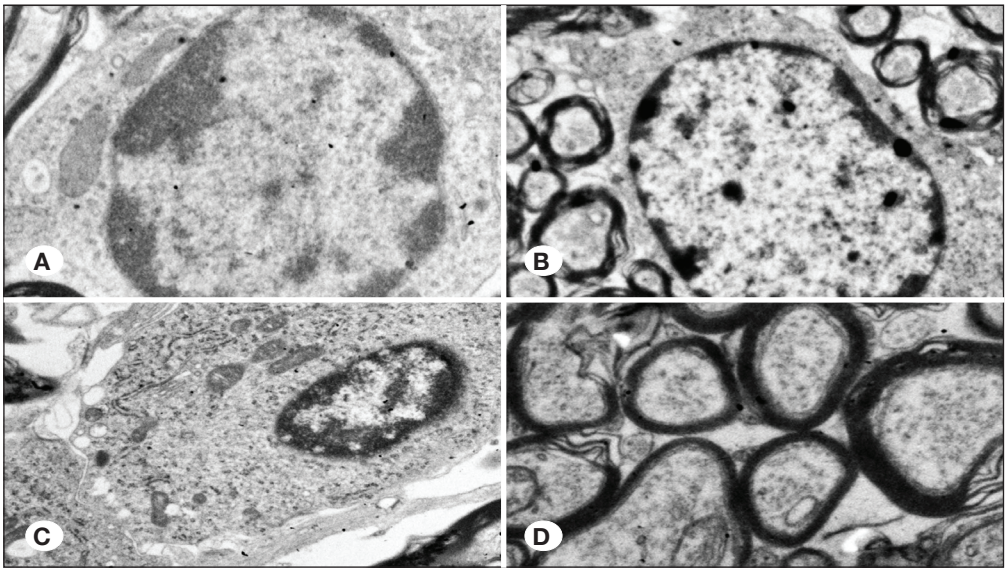

Figure 4: A, B) A round or oval euchromatic nucleus and an electron-dense nucleus. **C, D)** The myelin sheath and concentric rings around the axon. (x10000).

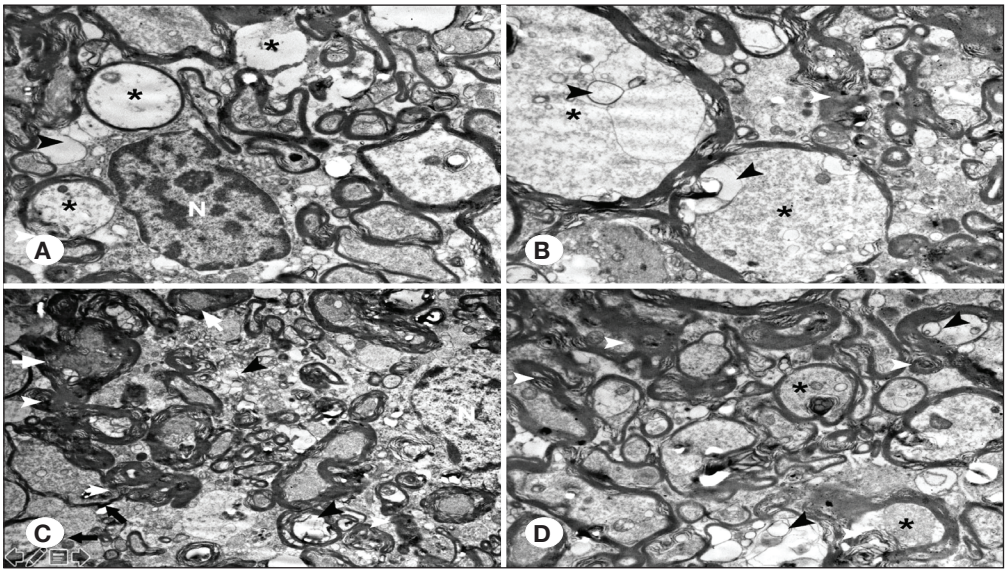

Figure 5: A) Myelin-induced thickened debris structures and loss of myelin (white arrow) in the optic chiasm, watery degeneration with axon swelling (black asterisks), and nucleus of oligodendrocyte (N). **B)** Thickened debris from myelin structures (white arrows) and lamelinization in axons (black asterisks) and vacuoles (black arrows). **C)** Dark axon degeneration (white arrows) and vacuoles (black arrow). **D)** Myelin-derived multilayered helical tubulovesicular structures (white arrow). (x7500).

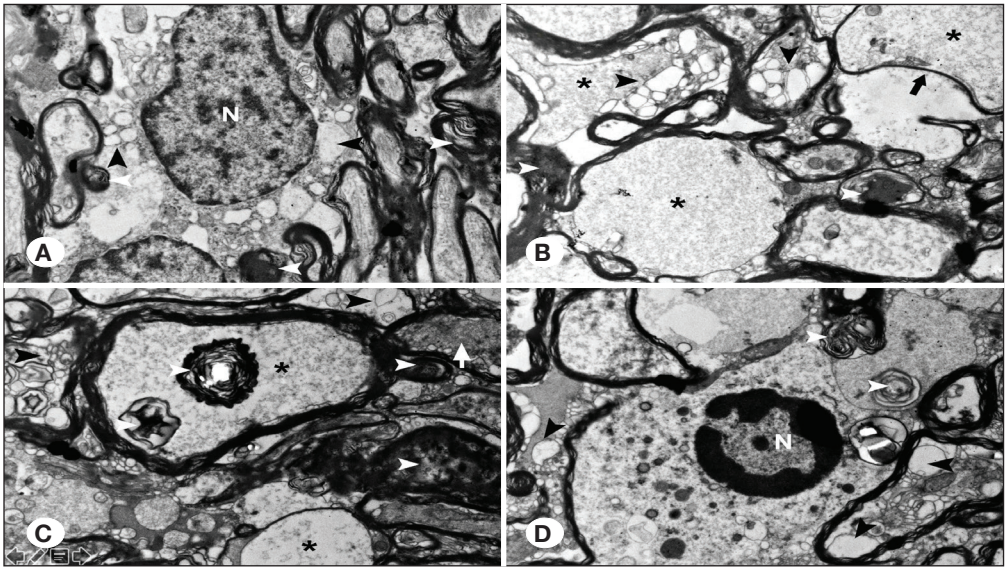

Figure 6: A) Degeneration of myelin debris (white arrows), excessive vacuolization of oligodendrocyte nucleus (N), and cytoplasm (black arrows). **B)** Degeneration of myelin debris (white arrow), loss of myelin and lamelization, and vacuoles (black arrow) in axons (asterisks). **C)** Dark axon degeneration (white arrow). **D)** Vacuoles (black arrow) and lymphocyte nucleus (N) in axons. (x10000).

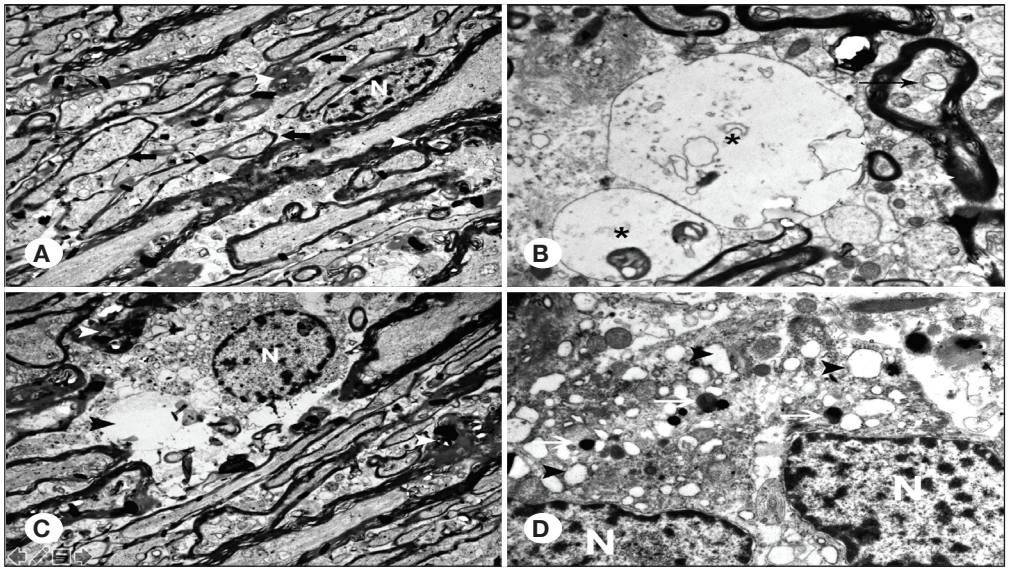

Figure 7: A) Myelin-derived debris structures (white arrow), myelin disorganization and loss, and microglia nucleus (N). **B)** Loss and lamelization of myelin and vacuoles (black arrow) in axons (asterisk). **C)** Excessive vacuolization and degeneration of myelin-derived debris structures (white arrow), oligodendrocyte nucleus (N), and cytoplasm. **D)** The nucleus of oligodendrocytes (N) and lipofuscin (white arrows) deposition. (x7500).

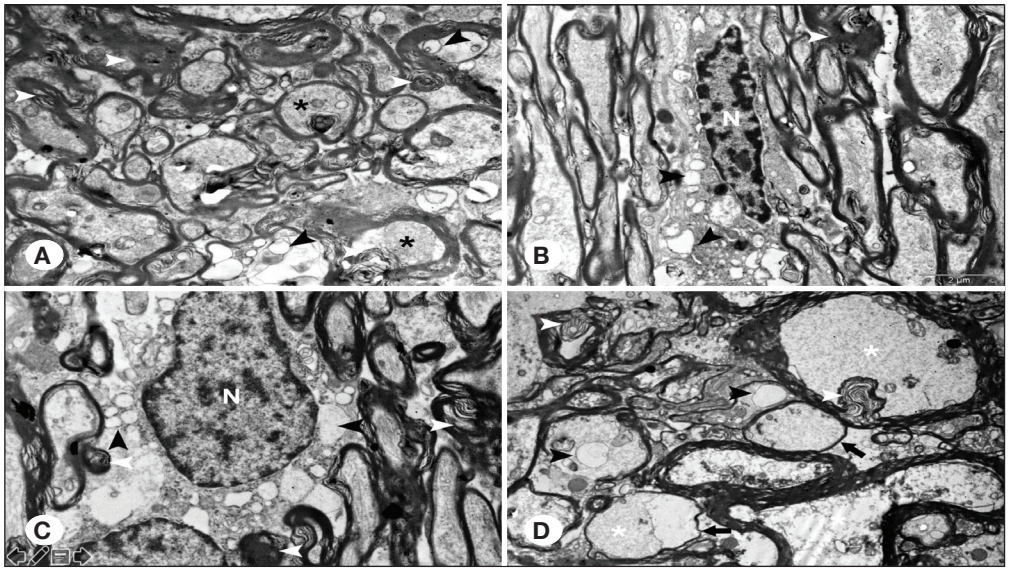

Figure 8: A) Myelin-derived multilayered helical tubulovesicular structures (white arrow) and vacuoles (black arrow) in axons (black asterisks). **B)** Degeneration of myelin debris (white arrow), vacuoles (black arrowheads), and nucleus (N) in axons and cytoplasm of microglia. **C)** Degeneration of myelin debris (white arrows), loss and lamelization of myelin, and excessive vacuolization of the cytoplasm (black arrows). **D)** Degeneration of myelin debris (white arrow), lamelization of myelin, and vacuoles (black arrow) in axons (asterisks). (x7500).

vacuolized irregularly shaped axons, excessively thickened myelin sheaths, and suffocated axons with a vacuolized periaxonal area. There were also severe delamination, demyelination, destruction, and loss of myelin lamellae and multiple swollen axon degenerations (watery degeneration). Large and excessive vacuolation, damaged mitochondria, and lipofuscin granule accumulation were observed in the cytoplasm of oligodendrocytes when compared with the control group. Elongated amoeboid (activated migrating) microglia may be found near oligodendrocytes. The microglia were characterized by a hypertrophic cytoplasm with vacuoles and an irregularly contoured and disoriented nucleus. Microglia exhibited an electron-dense nucleus and cytoplasm and an increase in extracellular space.

The severe compression remyelination group had severe disorganization of nerve fibers, vacuolized axons, myelin debris, and vacuolized axons (Figure 9). Multiple swollen axon degenerations resulted in an increase in extracellular space. When compared with the control and mild demyelination and remyelination groups, the number of oligodendrocytes was significantly reduced. Microglia had cytoplasm with vacuoles and irregularly contoured nuclei. Lymphocytes and erythrocytes were found in the extracellular space.

DISCUSSION

Although various models have been developed to exhibit optic demyelination, no remyelination model has been defined to exhibit chiasmal compression caused by tumoral lesions. There is a need to investigate the amount of recovery in the process of visual pathways after pituitary gland tumor surgery and patient-to-patient differences in optical remyelination. Our experimental model causes degeneration due to pressure while avoiding toxic and chemical agents from damaging the optic nerve. Thus, in electron microscopy examinations, our

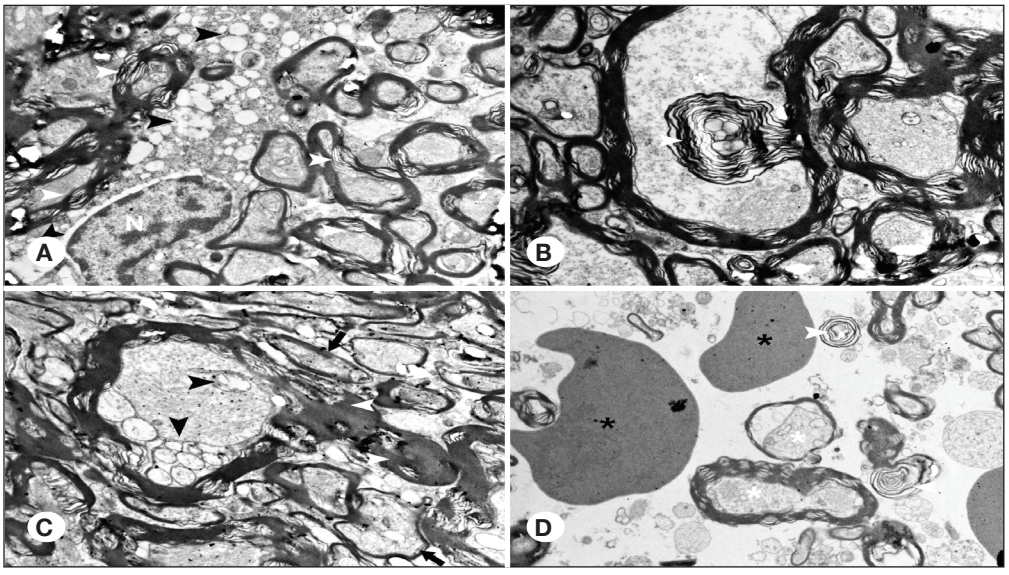

Figure 9: A) Degeneration and lamelization of myelin debris (white arrow), vacuoles (black arrow), and nuclei (N) in axons and cytoplasm of microglia. **B)** Degeneration of myelin debris (white arrowhead) in the axon (asterisk). **C)** Degeneration of myelin debris (white arrow) in the axon and vacuoles and lamelization. **D)** Degeneration of myelin debris (white arrow), vacuoles in axons (white asterisks), and erythrocytes (black asterisks). (x10000).

model can be used to study the pre-remyelination process following an episode of demyelination due to tumoral compression in all groups, except the control group. We expect the expected time for optic healing to be extended, so this is a preliminary study for new treatment protocols that will affect this process.

Pituitary macroadenomas cause vision loss by compressing the anterior visual pathways. Many prognostic factors (age, tumor size, duration of visual symptoms, secreting or non-secreting adenoma, and retinal nerve fiber layer problems) are defined for visual field defects and contribute to surgical decision-making for sellar region tumors (2,13,16,24,35). Initial axoplasmic flow disorder, conduction blockage, and demyelination are reversible functional mechanisms on the optic nerve in patients with pituitary apoplexy presenting with signs of acute vision loss (1,32), and significant improvements are often observed if early surgical decompression is performed (29). A reversible demyelination process allows for rapid recovery without the need for remyelination.

Visual improvement is believed to occur in two or three stages following surgical treatment (20). Improvement of nerve transmission begins in the early stage, which includes the first days after surgery, by relieving pressure on the visual pathways. The delayed recovery stage is caused by axonal transport and remyelination repair and is based on vascular structure recovery (13,18,20). Delayed surgery can cause irreversible axonal fiber degeneration in the optic nerve (32). These mechanisms are believed to play a significant role in nerve healing during the first 3 months (10).

The size of the tumor influences the degree of preoperative vision loss, duration of symptoms, and postoperative recovery. The primary surgical goal for giant adenoma is to provide maximum tumor resection and optic chiasm decompression with intracapsular debulking (6). Additionally, some researchers have shown that visual recovery is related to tumor size and duration of symptoms. Previous research had shown that tumor size was the most important factor influencing visual pathways and postoperative visual improvement was mostly observed in the first year (2,3).

VEP, optical coherence tomography (OCT), and diffusion tensor imaging (DTI) can be used to show the demyelination and remyelination processes in these optic nerves (27,34,36). In our clinic, the demyelination process was demonstrated using DTI in two studies showing optic nerve degeneration and remyelination in patients with visual loss due to sellar lesions (2,3). The results of this study indicate that demyelinated fibers can undergo remyelination following optical decompression and the first 1-yr period after the compression effect is removed is the most critical time interval in terms of axonal recovery (2).

The aim of our experimental model was to specifically target the optic chiasm with mechanical compression. All experimental groups showed Wallerian degeneration and myelin loss, except for the control group. Myelin debris was found in the extracellular space as a result of axonal loss. Other axons showed myelin changes, such as myelin delamination or enlargement, circular buds-bulges, and myelin tangles originating from the inner layers of myelin. Our compression model was used to achieve demyelination based on the results obtained in the experimental groups. Myelin debris was found in groups with mild demyelination and remyelination that had preserved intracellular organelles and nuclei. While the extracellular space increased in the severe compression groups, lymphocytes increased, and oligodendrocyte cells were absent in the severe remyelination group.

Previous studies found that the model caused by remyelination 4–5 weeks after optic damage but the remyelinated fibers did not reach their normal thickness and coexisted with demyelinated fibers (8,9). After mild and severe compression, remyelination was not observed, but oligodendrocyte cells were observed in the mild compression group. However, oligodendrocyte cells that would provide remyelination and

myelin formation in more than one axon could not be seen in EM examinations in the severe compression remyelination group. As a result, by allowing enough time for an increase in the number and activation of oligodendrocyte cells, it may be possible to show remyelination in mild compression groups after the compression is removed using this model. However, because the axonal damage in the severe compression group was irreversible, it was predicted that the remyelination process would not begin. Therefore, a longer follow-up period is required to allow for the remyelination process to begin after demyelination.

Demyelinating agents, such as lysolecithin, were used in stereotaxy experiments (15,31). However, demyelination caused by lysolecithin is due to the detergent-like effect of the toxin on myelin lipids rather than an immune-mediated inflammatory response. If the aim is to examine the demyelination and remyelination processes that occur after full tumoral compression, a mechanical compression model with a diffuse demyelination effect should be considered rather than a toxic and chemical agent with a focal effect (5,22).

Following the focal effect, all experimental groups showed Wallerian degeneration (rather than axonal degeneration). These degeneration mechanisms exhibit different remyelination processes. As a result, remyelination agents and treatments that promote axonal healing should perform differently in these degeneration mechanisms.

This technique, in which degeneration was induced solely by compressing the optic nerve without damaging it with toxic and chemical agents, clearly showed Wallerian degeneration caused by tumoral compression. In our opinion, this model will guide future experiments that will identify protocols to induce and accelerate remyelination.

CONCLUSION

The model used in this study showed histologically, using electron microscopy, the Wallerian degeneration observed under optic nerve compression. This is distinct from neurodegenerative disease degeneration. After the effect of compression is removed, this model allows for a better understanding of the optic nerve remyelination process, particularly in patients with pituitary macroadenoma. This experimental model can be used to develop new treatments and approaches.

ACKNOWLEDGEMENTS

Preparation for publication of this article is partly supported by Turkish Neurosurgical Society

AUTHORSHIP CONTRIBUTION

Study conception and design: AE, IA
Data collection: YA, IA
Analysis and interpretation of results: YA, AE, EBE
Draft manuscript preparation: AE, IA, EU
Critical revision of the article: IA, SuC, SC
Other (study supervision, fundings, materials, etc...): SK, AK, BC, MC
All authors (AE, IA, SK, AK, EY, EB, MC, YA, SuC, BC, SC) reviewed the results and approved the final version of the manuscript.

REFERENCES

1. Abdulbaki A, Kanaan I: The impact of surgical timing on visual outcome in pituitary apoplexy: Literature review and case illustration. Surg Neurol Int 8:16, 2017
2. Anik I, Anik Y, Cabuk B, Caklili M, Pirhan D, Ozturk O, Cirak M, Ceylan S: Visual outcome of an endoscopic endonasal transsphenoidal approach in pituitary macroadenomas: Quantitative assessment with diffusion tensor imaging early and long-term results. World Neurosurg 112:e691-e701, 2018
3. Anik I, Anik Y, Koc K, Ceylan S, Genc H, Altintas O, Ozdamar D, Ceylan DB: Evaluation of early visual recovery in pituitary macroadenomas after endoscopic endonasal transphenoidal surgery: Quantitative assessment with diffusion tensor imaging (DTI). Acta Neurochir (Wien) 153:831–842, 2011
4. Baumann N, Pham-Dinh D: Biology of oligodendrocyte and myelin in the mammalian central nervous system. Physiol Rev 81(2):871-927, 2001
5. Blakemore WF: Observations on remyelination in the rabbit spinal cord following demyelination induced by lysolecithin. Neuropathol Appl Neurobiol 4(1):47-59, 1978
6. Ceylan S, Sen HE, Ozsoy B, Ceylan EC, Ergen A, Selek A, Anik Y, Balci S, Cabuk B, Anik I: Endoscopic approach for giant pituitary adenoma: Clinical outcomes of 205 patients and comparison of two proposed classification systems for preoperative prediction of extent of resection. J Neurosurg 136(3):786-800, 2021
7. Chen Y, Wang C De, Su ZP, Chen YX, Cai L, Zhuge QC, Wu ZB: Natural history of postoperative nonfunctioning pituitary adenomas: A systematic review and meta-analysis. Neuroendocrinol 96:333–342, 2012
8. Clifford-Jones RE, Landon DN, McDonald WI: Remyelination during optic nerve compression. J Neurol Sci 46(2):239-243, 1980
9 Clifford-Jones RE, McDonald WI, Landon DN: Chronic optic nerve compression an experimental study. Brain 108:241-262, 1985
10. Dekkers OM, de Keizer RJW, Roelfsema F, vd Klaauw AA, Honkoop PJ, van Dulken H, Smit JWA, Romijn JA, Pereira AM: Progressive improvement of impaired visual acuity during the first year after transsphenoidal surgery for non-functioning pituitary macroadenoma. Pituitary 10:61–65, 2007

11. Fernández-Balsells MM, Murad MH, Barwise A, Gallegos-Orozco JF, Paul A, Lane MA, Lampropulos JF, Natividad I, Perestelo-Pérez L, Ponce de León-Lovatón PG, Erwin PJ, Carey J, Montori VM: Natural history of nonfunctioning pituitary adenomas and incidentalomas: A systematic review and metaanalysis. J Clin Endocrinol Metab 96:905–912, 2011
12. Foroozan R: Chiasmal syndromes. Curr Opin Ophthalmol 14(6):325-331, 2003
13. Gnanalingham KK, Bhattacharjee S, Pennington R, Ng J, Mendoza N: The time course of visual field recovery following transphenoidal surgery for pituitary adenomas: Predictive factors of a good outcome. J Neurol Neurosurg Psychiatry 76(3):415-419, 2005
14. Götz M, Huttner WB: The cell biology of neurogenesis. Nat Rev Mol Cell Biol 6(10):777-788, 2005
15. Hall SM: The effect of injections of lysophosphatidyl choline into white matter of the adult mouse spinal cord. J Cell Sci 10(2):535-546, 1972
16. Ismail M, Zidan W, Hamead K, Abdelhak B, Darwish M: Endoscopic transsellar transdiaphragmatic approach for extensive suprasellar pituitary macroadenomas. Am J Otolaryngol 42:102808, 2021
17. Jacobs DA, Galetta SL: Neuro-ophthalmology for neuroradiologists. AJNR Am J Neuroradiol 28(1):3-8, 2007
18. Jakobsson KE, Petruson B, Lindblom B: Dynamics of visual improvement following chiasmal decompression. Quantitative pre- and postoperative observations. Acta Ophthalmol Scand 80(5):512-516, 2002
19. Keirstead HS: Stem cells for the treatment of myelin loss. Trends Neurosci 28(12):677-683, 2005
20. Kerrison JB, Haller JA, Elman M, Miller NR: Visual field loss following vitreous surgery. Arch Ophthalmol 114(5):564-569, 1996
21. Kerrison JB, Lynn MJ, Baer CA, Newman SA, Biousse V, Newman NJ: Stages of improvement in visual fields after pituitary tumor resection. Am J Ophthalmol 130(6):813-820, 2000
22. Lachapelle F, Bachelin C, Moissonnier P, Nait-Oumesmar B, Hidalgo A, Fontaine D, Baron-Van Evercooren A: Failure of remyelination in the nonhuman primate optic nerve. Brain Pathol 15(3):198-207, 2005
23. Laws ER Jr, Trautmann JC, Hollenhorst RW: Transsphenoidal decompression of the optic nerve and chiasm. Visual results in 62 patients. J Neurosurg 46(6):717-722, 1977
24. Lee IH, Miller NR, Zan E, Tavares F, Blitz AM, Sung H, Yousem DM, Boland MV: Visual defects in patients with pituitary adenomas: The myth of bitemporal hemianopsia. AJR Am J Roentgenol 205(5):W512-518, 2015
25. Moon CH, Hwang SC, Kim BT, Ohn YH, Park TK: Visual prognostic value of optical coherence tomography and photopic negative response in chiasmal compression. Invest Ophthalmol Vis Sci 52(11):8527-8533, 2011
26. Moon CH, Hwang SC, Ohn YH, Park TK: The time course of visual field recovery and changes of retinal ganglion cells after optic chiasmal decompression. Invest Ophthalmol Vis Sci 52(11):7966-7973, 2011
27. Park JJ, Soetikno BT, Fawzi AA: Characterization of the middle capillary plexus using optical coherence tomography angiography in healthy and diabetic eyes. Retina 36:2039-2050, 2016
28. Peart JN, Headrick JP: Adenosinergic cardioprotection: Multiple receptors, multiple pathways. Pharmacol Ther 114(2):208-221, 2007
29. Rajasekaran S, Vanderpump M, Baldeweg S, Drake W, Reddy N, Lanyon M, Markey A, Plant G, Powell M, Sinha S, Wass J: UK guidelines for the management of pituitary apoplexy. Clin Endocrinol (Oxf) 74:9-20, 2011
30. Ralevic V, Burnstock G: Receptors for purines and pyrimidines. Pharmacol Rev 50(3):413-492, 1998
31. Shields SA, Gilson JM, Blakemore WF, Franklin RJ: Remyelination occurs as extensively but more slowly in old rats compared to young rats following gliotoxin-induced CNS demyelination. Glia 28(1):77-83, 1999
32. Singh TD, Valizadeh N, Meyer FB, Atkinson JLD, Erickson D, Rabinstein AA: Management and outcomes of pituitary apoplexy. J Neurosurg 122:1450–1457, 2015
33. Xie F, Liang P, Fu H, Zhang JC, Chen J: Effects of normal aging on myelin sheath ultrastructures in the somatic sensorimotor system of rats. Mol Med Rep 10(1):459-466, 2014
34. Yamada H, Yamamoto A, Okada T, Kanagaki M, Fushimi Y, Porter DA, Tanji M, Hojo M, Miyamoto S, Togashi K: Diffusion tensor imaging of the optic chiasm in patients with intra-or parasellar tumor using readout-segmented echo-planar. Magn Reson Imaging 34:654–661, 2016
35. Yoneoka Y, Hatase T, Watanabe N, Jinguji S, Okada M, Takagi M, Fujii Y: Early morphological recovery of the optic chiasm is associated with excellent visual outcome in patients with compressive chiasmal syndrome caused by pituitary tumors. Neurol Res 37:1–8, 2015
36. You Y, Gupta VK, Chitranshi N, Reedman B, Klistorner A, Graham SL: Visual evoked potential recording in a rat model of experimental optic nerve demyelination. J Vis Exp 101:e52934, 2015
37. Zhang SC, Ge B, Duncan ID: Adult brain retains the potential to generate oligodendroglial progenitors with extensive myelination capacity. Proc Natl Acad Sci U S A 96(7):4089-4094, 1999